The Astrophysical Journal Supplement Series, 271:4 (10pp), 2024 March https://doi.org/10.3847/1538-4365/ad1eeb

Projected Rotational Velocities for LAMOST Stars with Effective Temperatures Lower than 9000 K

Fang Zuo[1,2], A-Li Luo[1,2,3], Bing Du[1], Yinbi Li[1], Hugh R. A. Jones[4], Yi-han Song[1], Xiao Kong[1], and Yan-xin Guo[1]
[1] CAS Key Laboratory of Optical Astronomy, National Astronomical Observatories, Beijing 100101, People's Republic of China; lal@nao.cas.cn
[2] School of Astronomy and Space Science, University of Chinese Academy of Sciences, Beijing 101408, People's Republic of China
[3] University of Chinese Academy of Sciences, Nanjing, Jiangsu, 211135, People's Republic of China
[4] School of Physics, Astronomy and Mathematics, University of Hertfordshire, College Lane, Hatfield AL10 9AB, UK
Received 2023 November 1; revised 2023 December 29; accepted 2024 January 7; published 2024 February 12

Abstract

In Data Release 9 of LAMOST, we present measurements of $v \sin i$ for a total of 121,698 stars measured using the Medium Resolution Spectrograph (MRS) and 80,108 stars using the Low Resolution Spectrograph (LRS). These values were obtained through a χ^2 minimization process, comparing LAMOST spectra with corresponding grids of synthetically broadened spectra. Due to the resolution and the spectral range of LAMOST, $v \sin i$ measurements are limited to stars with an effective temperature ($T_{\rm eff}$) ranging from 5000 to 8500 K for MRS and 7000 to 9000 K for LRS. The detectable $v \sin i$ for MRS is set between 27 and 350 km s^{-1}, and for LRS between 110 and 350 km s^{-1}. This limitation is because the convolved reference spectra become less informative beyond 350 km s^{-1}. The intrinsic precision of $v \sin i$, determined from multiepoch observations, is approximately ∼4.0 km s^{-1} for MRS and ∼10.0 km s^{-1} for LRS at a signal-to-noise ratio greater than 50. Our $v \sin i$ values show consistency with those from APOGEE17, displaying a scatter of 8.79 km s^{-1}. They are also in agreement with measurements from the Gaia DR3 and Sun et al. catalogs. An observed trend in LAMOST MRS data is the decrease in $v \sin i$ with a drop in $T_{\rm eff}$, particularly transiting around 7000 K for dwarfs and 6500 K for giants, primarily observed in stars with near-solar abundances.

Unified Astronomy Thesaurus concepts: Astronomical techniques (1684); Stellar rotation (1629)

Supporting material: machine-readable table

1. Introduction

Measuring stellar rotation is of long-standing interest in stellar astrophysics. It is a key parameter for detecting the evolution of stellar angular momentum, which is advocated as the mechanism able to explain mixing and dilution (Nofi et al. 2021; Sun et al. 2021; Kounkel et al. 2023). Thus, knowledge of stellar rotation velocity may provide us a better understanding of stellar interior structure. In addition, the rotation period is an important parameter for gyrochronology, age dating using a star's rotation period and mass, which is mostly important for cool stars that evolve too slowly for isochrone dating to work (Lu et al. 2023).

Several methods have been used to determine projected rotational velocity ($v \sin i$) from spectroscopy. It can be obtained from the first zero frequency of the Fourier transform (FT) of the isolated spectral line profile (Smith & Gray 1976; Royer et al. 2002; Levenhagen 2014; Takeda 2020), or the cross-correlation function (CCF) technique (Melo et al. 2001). However, the two methods were not widely applied to large sky survey projects, because the FT technique needs high-resolution and high signal-to-noise ratio (S/N) spectra, and the CCF technique requires a calibrator with $v \sin i$ accurately determined by other techniques. One widely used method was proposed in Slettebak (1949), which use a rotational broadening function to generate a theoretical grid with different rotations, and determined $v \sin i$ of 125 brighter O, B2-B5, and B2e-B5e stars by comparing the observed line contours of He I 4026 Å to the theoretical line contours. Slettebak (1954, 1955) conducted subsequent measurement for several hundred stars ranging from B8 to G0, adhering to his previous method. In 1975, he further extended his research by obtaining $v \sin i$ measurements for 217 stars classified as O9-F9, which serve as a calibration standard for rotational velocities (Slettebak et al. 1975). This method has also been applied to determining the rotational velocities of cool stars with high-resolution spectra. (Delfosse et al. 1998) derived the $v \sin i$ values for 118 field M dwarfs, and Reiners & Basri (2008) determined the $v \sin i$ values for 45 L dwarfs.

As the $v \sin i$ values for an increasing number of stars were calculated, several interesting phenomena emerged. Slettebak (1949) discovered that Be stars have rotation velocities larger than those of typical B-type stars. Fukuda (1982) found that the Ae stars are faster rotators compared to typical A-type stars, and Burkhart (1979) found that chemically peculiar metallic-line (Am) stars are predominantly slow rotators. For dwarf stars, Kraft (1967) discovered the Kraft break around F0, and stars hotter than F0 have faster rotational velocities. The break was also discovered by later spectroscopic studies (Sun et al. 2019; Kamann et al. 2020). For giant stars, Gray (1989) found the rotational break occurs near G0. The reason for these observable variations may be that hot stars possess extremely thin convective envelopes, which prevent them from generating magnetic winds and causing angular momentum loss, while cold stars have thick convective envelopes, thus their slow rotation velocity is considered a

consequence of magnetic braking (Schatzman 1962; Kawaler 1988). It is known that stellar rotation is a complex physical process and large-sample rotational velocity catalogs from large sky surveys allow us to better understand the multifaceted nature of stellar rotation.

With the development of large sky surveys, data reduction pipelines were being developed to automatically measure stellar parameters. The Apache Point Observatory Galactic Evolution Experiment (APOGEE) developed the APOGEE Stellar Parameter and Chemical Abundances Pipeline (ASPCAP) for the automated analysis of high-resolution spectra (R ∼22,500 across 15100–15799 Å, 15867–16424 Å, and 16484–17000 Å) of the stars across the Milky Way (García Pérez et al. 2016). ASPCAP determines atmospheric parameters ($T_{\rm eff}$: effective temperature, log g: surface gravity, and [M/H]: metallicity) and chemical abundances by comparing observed spectra to grids of synthetic spectra, minimizing χ^2 in a multidimensional parameter space. In the 16th data release (DR), a projected rotational velocity dimension was added to the the dwarf subgrids (log $g < 2.5$ dex), and the v sin i of dwarfs were determined by ASPCAP (Jönsson et al. 2020).

Gaia DR3 obtained the projected rotational velocities from the by-product of Extended Stellar Parametrizer for Hot Stars (ESP-HS), measuring the line broadening on the radial velocity spectrometer (RVS) spectra (8450–8720 Å). However, despite the relatively high resolution (R ∼ 11,500), ESP-HS values suffer from poor v sin i –related information for hot stars such as OBA types due to the relatively limited wavelength range (Fouesneau et al. 2023).

Similar to other large sky surveys, the Large Sky Area Multi-Object Fiber Spectroscopic Telescope survey (LAMOST; Wang et al. 1996; Su & Cui 2004; Zhao & Newberg 2006; Cui et al. 2012; Zhao et al. 2012) developed the LAMOST stellar parameter pipeline (LASP) to automatically determine stellar parameters by analyzing Low-Resolution Spectrograph (LRS) spectra, covering the wavelength range of 3800–9000 Å with a resolution of R ∼ 1800 (Luo et al. 2015). Since the LAMOST-II Medium-Resolution Spectrograph (MRS) survey, the LASP was adapted to the MRS spectra (4950–5350 Å and 6300–6800 Å, R ∼7500). We updated LASP by adding a method to measure projected rotational velocity from the LAMOST spectra, using the synthetic spectra of PHOENIX (Husser et al. 2013). The updated LASP was developed to obtain a projected rotational velocity when other parameters were determined. The updated LASP was applied to the LAMOST DR9 and here provides a catalog of 121,698 rotational velocities for MRS stars and for 80,108 LRS targets.

In this paper, we provide a thorough description of the v sin i measurement in the updated LASP. This paper is organized as follows. Section 2 details the data we used in this work. Section 3 describes the method we adopted, its validation on APOGEE spectra and application to LAMOST spectra. Section 4 displays the results of this work and displays external accuracy by comparisons with catalogs. Finally, we summarize this work in Section 5.

2. Data

2.1. PHOENIX Grids

In this study, version 16 of PHOENIX was adopted (Husser et al. 2013), which used a new equation of state and an up-to-date atomic and molecular line list. This allowed PHOENIX to produce synthetic spectra that match observations better than other synthetic libraries, especially for cool stars.

Table 1
Parameter Ranges of the PHOENIX Subgrids Used in This Work

	Range	Step Size
$T_{\rm eff}$ (K)	2300–7000	100
	7000 –12,000	200
log g (dex)	0–6.0	0.5
[Fe/H] (dex)	−4.0 to −2.0	1.0
	−2.0 to +1.0	0.5

The synthetic spectra cover the wavelength range from 500 Å to 5.5 μm in the optical and near-IR, with a resolution of $R \sim 500{,}000$. The grid coverage of $T_{\rm eff}$ is from 2300–12,000 K, log g from 0.0–6.0 dex, and metallicity ([Fe/H]) from −4.0 to 1.0 dex. We did not take into account alpha enhancement in this work, and selected the subgrids of $[\alpha/{\rm Fe}] = 0.0$, which are listed in Table 1.

2.2. Preliminary Sample Selection

The LAMOST DR9 collected more than 3 million (1.4 million stars) MRS and 10 million (7.6 million stars) LRS spectra, of these, 0.8 million stars with 1.6 million MRS spectra were parameterized by the LASP and 5.1 million stars with 7 million LRS spectra were parameterized for LRS. LASP has the equivalent accuracies of stellar parameters on both MRS and LRS, which are about 100 K, 0.19 dex, and 0.10 dex for $T_{\rm eff}$, log g, and [Fe/H], respectively, in the effective temperature range of 4000 K $< T_{\rm eff} <$ 8500 K (Luo et al. 2015). This is because the MRS, despite its higher resolution, covers a very small wavelength range, from 4950–5350 Å for the blue band, and 6300–6800 Å for the red band. However, LASP can derive a higher precision radial velocity (RV) for MRS than LRS, with a precision of ∼1.5 km s^{-1} compared to ∼5.0 km s^{-1} (Luo et al. 2015; Wang et al. 2019).

Considering the wavelength coverage of the MRS, we selected stars with 5000 K $< T_{\rm eff} <$ 8500 K to determine v sin i from the coadded spectra. We had no confidence in the parameters of stars with $T_{\rm eff}$ >8500 K, because there is no Balmer line in the blue part of the MRS spectrum that LASP used. For the LRS, the low resolving power ($R \sim 1800$) allows us to detect only fast-rotating stars, but fast-rotating stars are rare in the late-type stars. Therefore, we abandoned the late-type stars and added a few early-type stars, which are in the effective temperature range of 7000 K $< T_{\rm eff} <$ 9000 K.

In addition, both MRS and LRS observations have a nearly fixed instrumental profile with a mean full width at half maximum (FWHM) of $\mu = 0.68$ Å for MRS (see Figure 1) and a mean FWHM of $\mu = 3.04$ Å for LRS (see Figure 2), with a scatter of 0.06 Å for MRS and 0.11 Å for LRS. This indicates that resolutions of MRS and LRS vary with wavelength; such a resolution variation has an impact on the v sin i, and we abandoned fibers with FWHMs beyond 2σ.

Nonsingle targets were also removed from samples previously selected through crossmatching with Gaia DR3 (Gaia Collaboration et al. 2021), and the catalogs from Whiting et al. (2023) and Penoyre et al. (2022), which offered nearby binaries, Stars with RUWE > = 1.4, and ipd_gof_harmonic_amplitude < 0.1

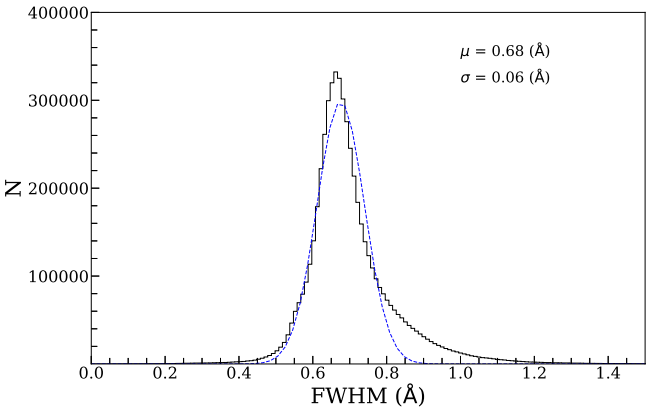

Figure 1. Histogram of the full width at half maximum (FWHM) of the thorium–argon wavelength calibration lines for MRS. The blue curve is the Gaussian fit to the FWHM distribution.

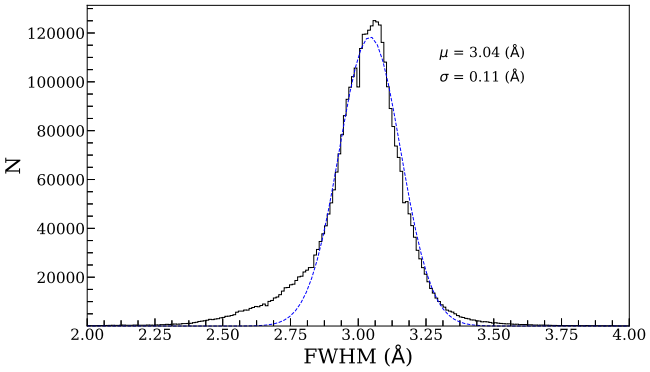

Figure 2. Histogram of the FWHM of the arc calibration lines for the LRS with the best-fit Gaussian plotted in blue.

or ipd_frac_multi_peak < 10 (El-Badry et al. 2021) were also cut out.

3. Method

In this work, we used χ^2 minimization in the v sin i space to derive the best-matched v sin i under the constraints of other parameters.

3.1. The Determination Method of v sin i

There are four steps for v sin i determination, including generation of the reference spectrum by interpolating PHOENIX grids, matching of spectral resolution, convolution of the broadening kernel, and χ^2 minimization.

1. *Generation of the synthetic reference spectrum*. Since the atmospheric parameters have already been determined by LASP, we generated the reference spectrum by linearly interpolating the PHOENIX grids with atmospheric parameters around the LASP-determined ones.
2. The resolution of generated reference spectrum was reduced to the resolution of the observed spectrum.
3. *Convolution of the broadening kernel*. The broadening kernel was taken from Gray (2005) and is given below:

$$\delta = 1 - \left(\frac{v}{n}\right)^2, \tag{1}$$

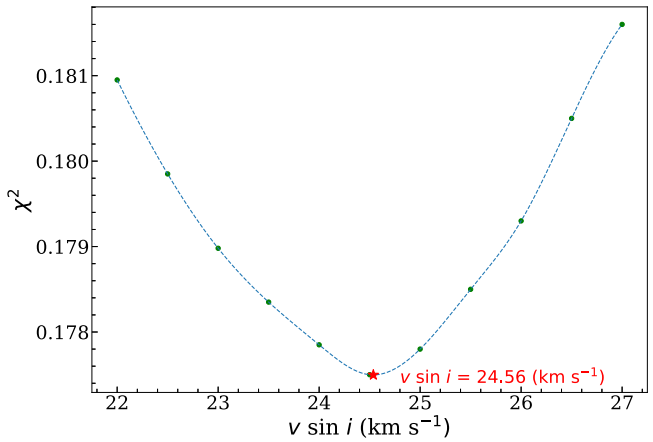

Figure 3. An example χ^2 minimization curve showing the fitting process. The blue dashed curve is the result of dense-spline interpolation, and the red asterisk is the minimum χ^2 point.

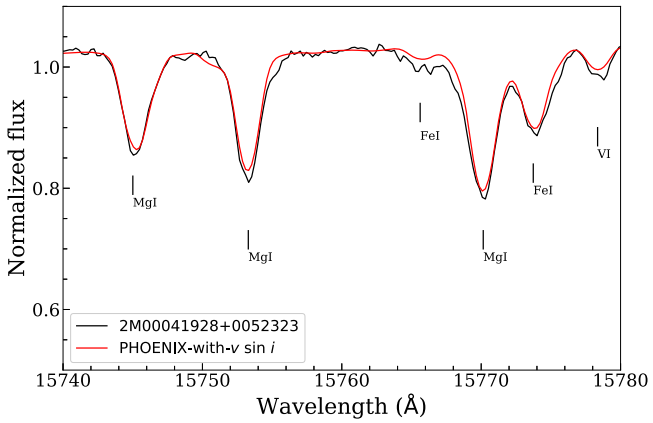

Figure 4. An example APOGEE spectrum is plotted in black along with a best-fit model spectrum in red. The ASPCAP parameters of this target are $T_{\rm eff} = 6188.34$ K, $\log g = 4.2$ dex, and $[{\rm Fe/H}] = -0.01$ dex. The reference spectrum from PHOENIX includes rotational velocity broadening of 13.3 km s^{-1}.

$$G(\delta) = \frac{2(1-\varepsilon)\delta^{1/2} + \frac{1}{2}\pi\varepsilon\delta}{\pi n(1-\varepsilon/3)}, \tag{2}$$

where v is the rotational velocity v sin i, ε is the limb-darkening coefficient, n is the width of the convolutional kernel, and its value is resolution dependent. We adopted $\varepsilon = 0.6$, $n = 7$ for MRS and $n = 75$ for LRS, and we produced 700 spectra with different v sin i through convolving the reference spectrum with different rotational kernels from v sin $i = 1$ km s^{-1} to 350 km s^{-1} (step $= 0.5$ km s^{-1}).

4. χ^2 *minimization*. We minimized χ^2 by comparing the observed spectrum to the convolved reference spectra. Then we fitted the 11 points of (v sin i, χ^2) which have the minimum χ^2 in the middle (see the blue points in Figure 3), using a dense-spline interpolation method instead of a Gaussian to avoid fitting failure (Du et al. 2019). The minimum χ^2 point of the dense interpolation corresponds to the projected rotational velocity of the observed spectrum (see the red star in Figure 3).

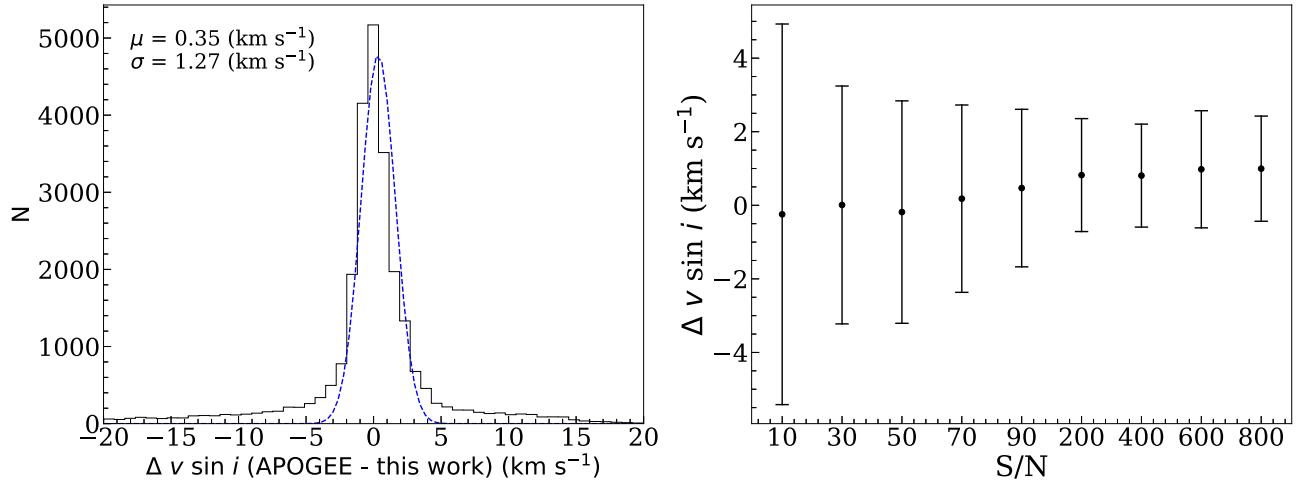

Figure 5. Comparison of our v sin i results with those from ASPCAP. The left panel shows the histograms of differences between results of this method and those of ASPCAP along with a Gaussian fit in blue. The right panel shows the distribution in v sin i values as a function of the signal-to-noise ratio (S/N).

3.2. Validation on the APOGEE Spectra

To validate our method, we performed the method on APOGEE spectra with a resolution of $R \sim 22{,}500$. The APOGEE spectra included three bands, [15100–15799 Å], [15867–16424 Å], and [16484–17000 Å], and we used the spectrum of 15740–15780 Å, where four strong isolated lines exist (see Figure 4) to measure v sin i.

Because of the resolution of APOGEE spectra, stars rotating faster than 8 km s^{-1} can be detected (Frasca et al. 2016). We selected the sample from the APOGEE DR17 catalog with the ASPCAP $T_{\rm eff} > 5000$ K and a v sin i greater than 8 km s^{-1}, and finally a sample of 27,000 spectra were selected.

We determined v sin i for the 27,000 spectra and compared our results with the v sin i of ASPCAP, which is shown in Figure 5. The results of our method are consistent with those of ASPCAP, with a scatter of 1.27 km s^{-1}. To inspect the influence of S/N on the v sin i measurement, we calculated the mean and the standard deviation of the difference between our results and those of ASPCAP under different S/Ns (see the right panel in Figure 5), and noticed that the v sin i measurement is greatly affected by the S/N for S/N < 30, and less affected by S/N > 50.

We degraded the resolution of APOGEE spectra to $R = 7500$, to evaluate the performance of the spectra with the same resolution of LAMOST, and the result shows that the LAMOST MRS resolution allows us to detect only stars rotating faster than 27 km s^{-1}. We further excluded samples with the ASPCAP v sin i less than 27 km s^{-1} in the evaluation, Figure 6 shows the comparison of our results to the ASPCAP v sin i, and the difference has a scatter of 8.79 km s^{-1}.

3.3. Application to LAMOST

In this work, we estimated v sin i for both MRS and LRS in LAMOST DR9, using the blue-band spectra with 4950–5300 Å for MRS and 4200–5700 Å for LRS. The application of v sin i measurements to both surveys will be described below.

3.3.1. Application to the MRS

Consistent with the spectral band used in LASP, we also used the blue-arm spectra (4950–5300 Å) to measure v sin i, without using the red arm because of the possible existence of strong Hα emission (Wang et al. 2019). We adopted the stellar parameters of LASP, including $T_{\rm eff}$, log g, [Fe/H], and RV, and interpolated the synthetic spectra of the PHOENIX grids based on the LASP $T_{\rm eff}$, log g, and [Fe/H]. Then, we degraded the resolution of a reference spectrum to the resolution of MRS, and subtracted pseudocontinua of both the synthetic and the observed spectrum by polynomial fitting. We added the broadening kernel that was given in Section 3.1 to the synthetic spectrum (see Figure 7), and v sin i is determined by minimizing χ^2.

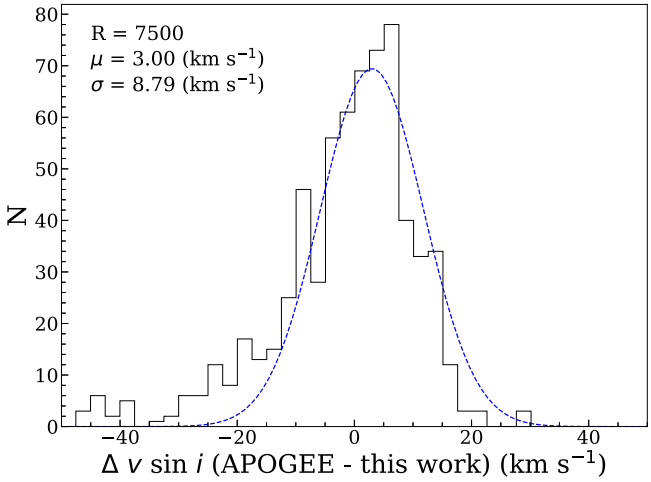

Figure 6. The histogram of the difference between our results and those of ASPCAP is shown along with a Gaussian fit in blue.

3.3.2. Application to the LRS

For the LRS, we used the spectra of 4200–5700 Å to determine v sin i. We did not use the Hα (6520–6595 Å) band because of its instability and that an RV offset of ~7 km s^{-1} exists in this band (Du et al. 2019). We did not take into account the Ca II triplet (8400–8700 Å), because the lines are weak for hot stars. Otherwise the measurement procedure for the LRS was consistent with that for the MRS.

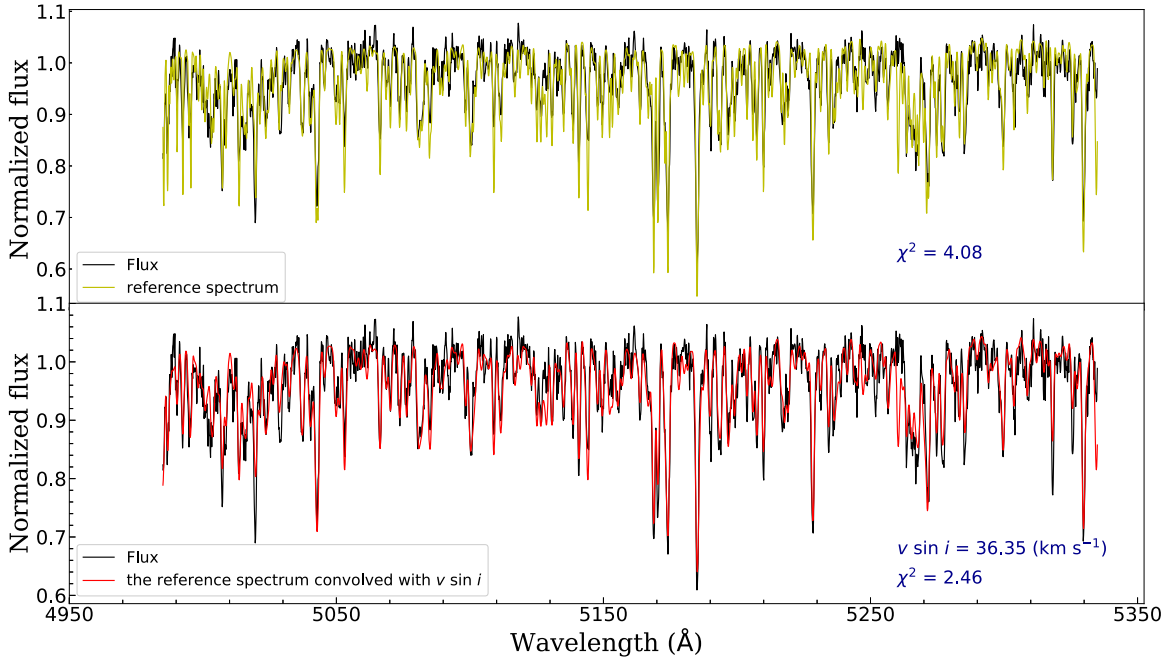

Figure 7. A comparison between an MRS spectrum in black with its best-fit model spectrum in yellow and red. The upper plot shows the model spectrum in yellow prior to broadening. The lower plot shows the synthetic spectrum following convolution with a suitable v sin i.

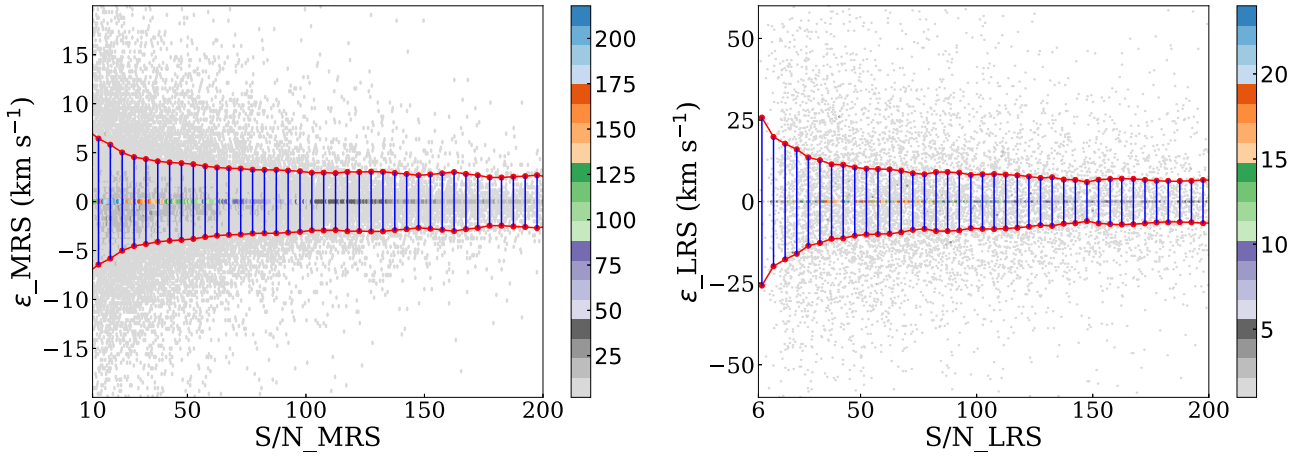

Figure 8. The distribution of v sin i precision at different S/Ns for MRS (left) and LRS (right). The color contours indicate the number of stars, and the red curves are the spline fits to the 1σ uncertainties of ϵ with an S/N step of 5.

4. Results

4.1. Precision

We estimated v sin i precision from the v sin i measurements of the multiple observations for the same stars (Du et al. 2021). The targets with more than three measurements were selected for the calculation, and the statistical estimator used to assess the precision is:

$$\epsilon = \sqrt{(n/(n-1))} \times (v \sin i_{\rm i} - \overline{v \sin i}) \quad (3)$$

where n is the observation times of the same star, v sin $i_{\rm i}$ is the v sin i of the ith observation, $i = 1, 2, ..., n$, and $\overline{v \sin i} = \frac{1}{n}\sum_{i=1}^{n} v \sin i_{\rm i}$.

Figure 8 shows the distribution of v sin i precision at different S/Ns for MRS and LRS. For both of them, v sin i precisions are highly dependent on the S/Ns when S/N < 50, while a fixed level of about 4.0 km s^{-1} as S/N < 50 is obtained for MRS and about 10.0 km s^{-1} when S/N > 50 for LRS.

4.2. Catalog

We construct two v sin i catalogs for LAMOST MRS and LRS, i.e., LAMOST MRS v sin i CATALOG and LAMOST LRS v sin i CATALOG, which include 121,698 stars (221,770 spectra) for MRS and 80,108 stars (102,598 spectra) for LRS respectively. The format for both MRS and LRS are the same and here we display some example lines of the MRS v sin i CATALOG in Table 2. The two full catalogs can be accessed at doi: 10.12149/101316. For the LAMOST MRS v sin i CATALOG, we did not have confidence in v sin i < 27 km s^{-1} as mentioned in Frasca et al. (2016), stars with v sin i < 27 km s^{-1} were removed, and for LAMOST LRS v

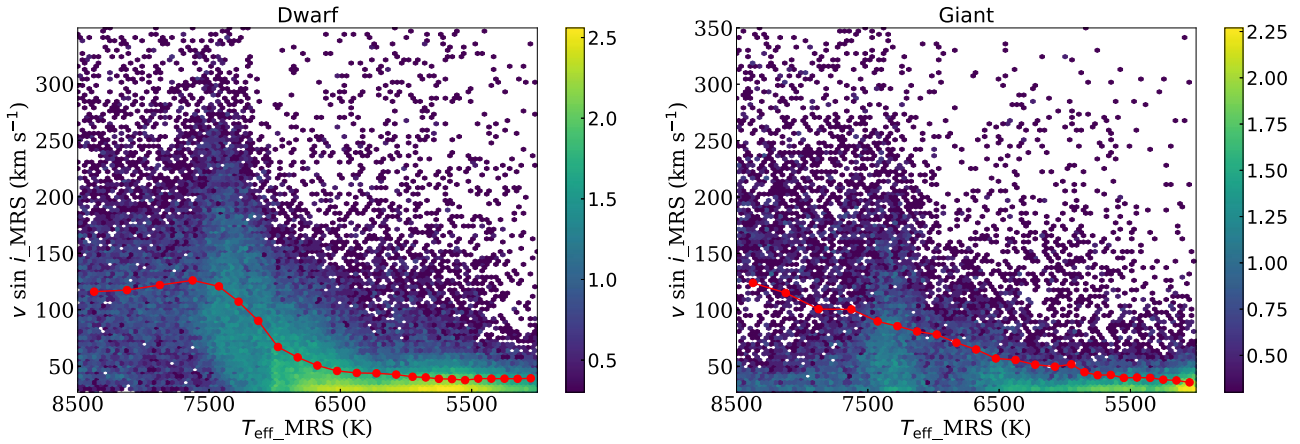

Figure 9. The v sin i –$T_{\rm eff}$ diagrams for dwarf stars (left) and giant stars (right), color coded by the log10 (number). The red curves are the spline fits to the average v sin i within nonuniform $T_{\rm eff}$ bins.

Table 2
Parameters of LAMOST MRS v sin i CATALOG

UID[a]	R.A. (deg)	Decl.	S/N	$T_{\rm eff}$ (K)	log g	[Fe/H] (dex)	v sin i[b]	v sin i_err[c] (km s^{-1})
G16865597923189	22.4280930	54.7624245	40	7662	3.98	0.14	224	2
G16865927110078	26.0557060	54.3317642	42	7850	3.91	0.02	90	4
G17457893282113	83.7000580	42.1455650	266	8135	4.02	−0.19	130	1
G17462346236306	75.8974991	48.2667503	114	7570	4.03	−0.05	113	1
G13295087724001	340.1962585	24.3700695	150	7473	3.91	0.27	45	4
G13292221927576	344.4146423	32.3737564	181	7919	4.09	0.01	92	2
G13296262504355	340.7543030	27.2950096	178	7527	4.15	−0.16	262	1
G13302953250167	356.0117493	29.4897861	158	7911	4.14	−0.14	118	1
G13307681691870	351.3109436	24.0695324	306	7672	4.01	0.21	94	2
G13278647737207	354.9405212	39.4682617	370	7702	3.94	0.07	58	2

Notes. The LAMOST LRS v sin i CATALOG has the same format, so we did not display it.
[a] LAMOST unique target ID.
[b] Projected rotational velocity derived with the method in this work.
[c] Error estimated by the method laid out in Section 4.1.

(This table is available in its entirety in machine-readable form.)

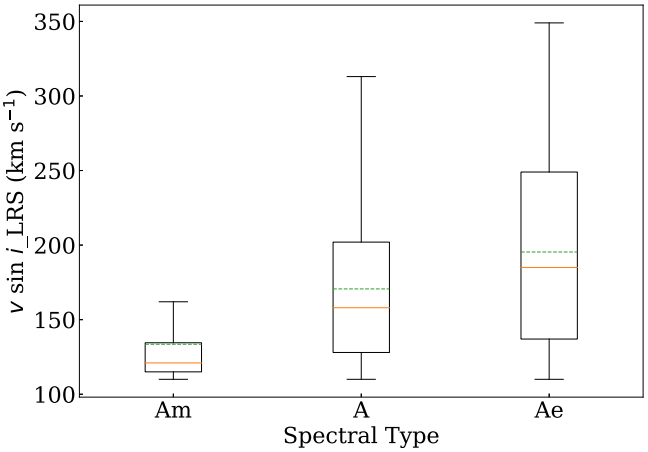

Figure 10. The box extends from the lower to upper quartile values of the LRS v sin i of Am, A, and Ae stars, with the green dashed (orange) line at the mean (median). The vertical lines extend from the boxes to show the v sin i range.

sin i CATALOG, stars with v sin i $< 110\,{\rm km\,s^{-1}}$ were removed for the same reason. Finally, 121,698 stars are included in the LAMOST MRS v sin i CATALOG, 80,108 stars for the LAMOST LRS v sin i CATALOG, and for stars with multiple observations, v sin i and uncertainties calculated from the spectrum with the highest S/N were given in the two catalogs.

The behaviors of rotation along the main sequence and giants were studied by Kraft (1967) and Gray (1989); stars with near solar abundances ($-0.5 \leqslant$ [Fe/H] $\leqslant 0.5$ dex) in the LAMOST MRS v sin i CATALOG were separated into dwarfs as log $g \geqslant 4.0$ dex and giants as log $g < 4.0$ dex so as to inspect their behaviors. We did not take into account the LAMOST LRS v sin i CATALOG because of its limited temperature range of $7000\,{\rm K} < T_{\rm eff} < 9000\,{\rm K}$. Figure 9 shows the distribution of v sin i at different temperatures; it sharply decreases at $T_{\rm eff} \sim 7000\,{\rm K}$ for dwarfs, which is consistent with the Kraft break around F0; the average rotational velocity of stars with $T_{\rm eff} < 7500\,{\rm K}$ (see the red curve in the left panel of Figure 9) is greater than $120\,{\rm km\,s^{-1}}$, which is similar to the result in Fukuda (1982). For giants, the break occurs at $T_{\rm eff} \sim 6500\,{\rm K}$, which is consistent with the rotation behavior in Burkhart (1979) and Gray (1989), and their average v sin i is larger than $50\,{\rm km\,s^{-1}}$, which indicates that giant stars have a gentle v sin

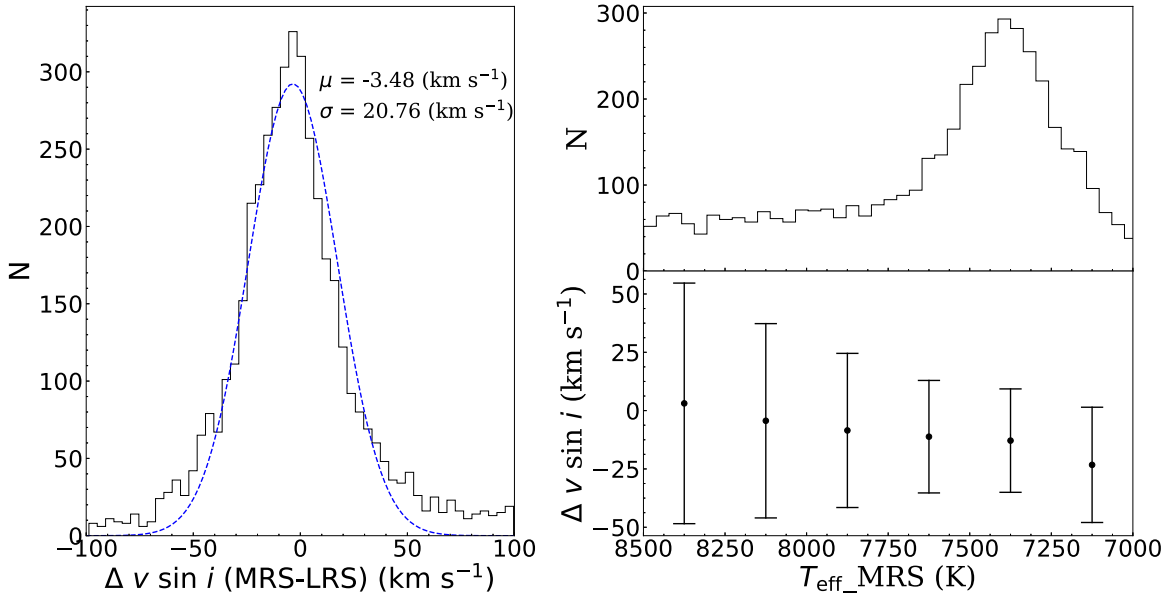

Figure 11. Comparison of the results between MRS and LRS data. The distribution of v sin i differences between the MRS and LRS is shown in the left panel. The upper right panel shows the number of v sin i values from the MRS LASP as a function of $T_{\rm eff}$. The distribution of v sin i differences between the MRS and LRS at different temperatures is shown in the lower right panel.

i transition (as shown by the red curve in the right panel of Figure 9).

As mentioned in the Introduction, compared to typical A-type star, Am and Ae are slower and faster rotators, respectively. We crossmatched the v sin i LRS CATALOG with the catalogs of Shang et al. (2022) (Am stars), "LAMOST Spectral Index of A type Stars," and Zhang et al. (2022) (Ae stars), and obtained 387 Am, 49,107 typical A-type (removed Am and Ae), and 2215 Ae stars. The rotational velocities of the three types of stars are shown in Figure 10, and their average v sin i are 121 km s^{-1}, 158 km s^{-1}, and 185 km s^{-1}, respectively, which are in agreement with the results in Fukuda (1982). We did not consider the MRS v sin i CATALOG here, because $T_{\rm eff}$ in this catalog are all lower than 8500 K, which means no hot A-type stars can be used.

4.3. Comparison of MRS and LRS

We crossmatched the LAMOST MRS v sin i CATALOG with the LAMOST LRS v sin i CATALOG, finding 6000 stars in common, which are all fast-rotating stars because the LAMOST LRS v sin i CATALOG only provides v sin $i < 110$ km s^{-1}. The difference distribution of v sin i for these stars is shown in Figure 11, with a mean of 3.45 km s^{-1} and a standard deviation of 20.76 km s^{-1}; the relative error of difference is less than 2%.

The v sin i differences at different temperatures are shown in Figure 11 (lower right panel), and we found that the differences become larger at $T_{\rm eff} > 8000$ K when compared to $7000 < T_{\rm eff} < 8000$ K, which is because the higher the temperature, the weaker the spectral lines of MRS blue-arm spectra are (4950–5300 Å). We noted a slight downward trend in the lower right panel of Figure 11; this is probably because the mixing of metal lines intensifies with the decrease of temperature for LRS, resulting in a whole overestimate of rotational velocity, which is why we did not measure v sin i for stars with $T_{\rm eff} < 7000$ K.

4.4. Comparison with Other Catalogs

To verify the reliability of the v sin i obtained from our method, we compared our results to other catalogs, including APOGEE DR17, Gaia DR3, and SUN (Sun et al. 2021, hereafter SUN), where APOGEE DR17 focuses on F-, G-, and K-type stars, while Gaia DR3 and SUN focus on early-type stars (F and A types). In order to reduce the uncertainty introduced by the stellar parameters, we selected the stars with temperature differences less than 500 K, and differences of both log g and [Fe/H] less than 1.0 dex.

4.4.1. Comparison with APOGEE DR17

Projected rotational velocities released in APOGEE DR17 are less than 100 km s^{-1}, which have no overlap with the LAMOST LRS v sin i CATALOG, thus we only compare the LAMOST MRS v sin i CATALOG with APOGEE DR17, and obtain 311 common stars. Figure 12 shows the comparison results, and we notice that v sin i given in this work are consistent with ASPCAP results, with a small offset of 0.40 km s^{-1}, and a scatter of 3.10 km s^{-1}.

4.4.2. Comparison with Gaia DR3

Gaia is a space mission of the European Space Agency (ESA) that started in 2013 (Gaia Collaboration et al. 2016), and the first data was released in 2016 (Clementini et al. 2016; Recio-Blanco et al. 2016). Its aim is to primarily provide a three-dimensional map of the Milky Way. In 2023, Gaia published DR3 (Creevey et al. 2023), including radii, masses, ages, chemical abundances, and more than 470 million stellar parameters ($T_{\rm eff}$, log g, and [Fe/H]). For hot stars, ESP-HS determined rotation velocities by measuring line broadening on RVS spectra (Fouesneau et al. 2023).

We crossmatched the LAMOST MRS v sin i CATALOG and LAMOST LRS v sin i CATALOG with Gaia DR3, and

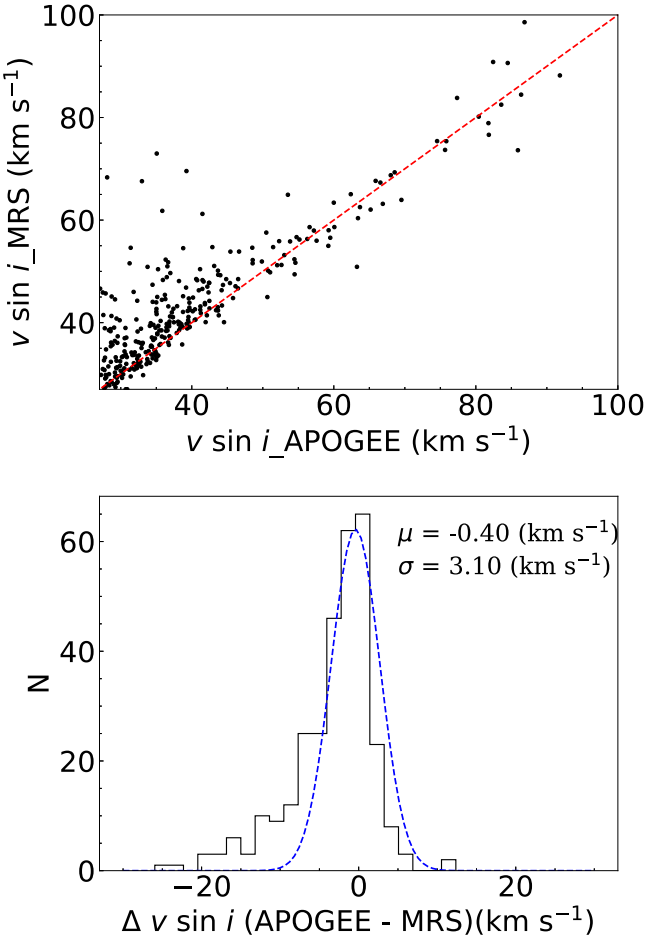

Figure 12. Comparison of MRS v sin i results in this work to APOGEE DR17, with the red line showing the one-to-one line. The lower plot shows the histogram of v sin i differences between the two catalogs with a Gaussian fit in blue.

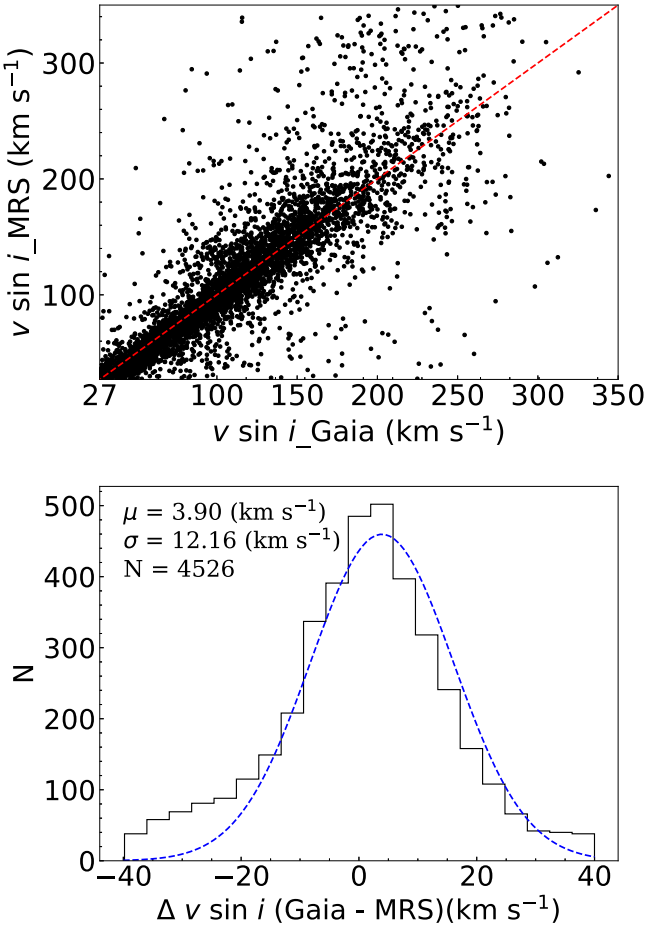

Figure 13. Comparison of MRS v sin i results in this work to Gaia DR3 following the conventions of Figure 12.

obtained 4526 common stars for MRS and 7013 common stars for LRS. Figure 13 shows the comparison between the MRS catalog and Gaia DR3 catalog, and Figure 14 shows the comparison of the LRS catalog to the Gaia DR3 catalog. The results in this work generally agree with Gaia v sin i with scatters of 12.2 and 24.7 km s^{-1} for MRS and LRS, respectively. The scatter of MRS is relatively larger than that of APOGEE DR17 (3.10 km s^{-1}), because ESP-HS only provided v sin i for hot stars, and v sin i–related information for hot stars in the 8450–8720 Å wavelength range is poor (Fouesneau et al. 2023).

4.4.3. Comparison with SUN

Sun et al. (2021) used a machine-learning algorithm to obtain stellar rotation, which trained a model with the theoretical Kurucz spectra, and it was used to calculate the v sin i of observed spectra.

We crossmatched the LAMOST MRS v sin i CATALOG and LAMOST LRS v sin i CATALOG with the SUN catalog (Sun et al. 2021), and obtained 8267 and 2628 common stars, respectively. We compared the results in the two LAMOST catalogs with those in SUN, which are shown in Figures 15 and 16. The offset and scatter between LAMOST MRS and SUN are 2.2 and 6.5 km s^{-1}, and 1.2 and 28.4 km s^{-1} for LRS and SUN, which indicates that the results are consistent and that the LRS has relatively large scatter.

5. Summary

In this work, we used χ^2 minimization to derive the best-matched v sin i under the constraints of atmospheric parameters determined by LASP, through comparing the observed spectra to the PHOENIX synthetic spectra. We validated this method on APOGEE DR17, integrated it into LASP, and applied it to LAMOST MRS and LRS spectra. Eventually, we obtained v sin i catalogs for both MRS and LRS.

1. *The v sin i determination method.* We used a minimum χ^2 algorithm to calculate v sin i through comparing the observed spectrum with the reference spectra from PHOENIX grids based on the atmospheric parameters that have already been determined by LASP. We first generated the synthetic reference spectrum with the theoretical PHOENIX grids and decreased the reference spectrum resolution to the observed spectrum resolution. Then, the reference spectrum was convolved by the broadening kernel with different v sin i taken from Gray (2005), and we finally obtained v sin i by the minimum χ^2 between the observed spectrum and those convolved reference spectra.
2. *Method validation.* We selected 27,000 APOGEE DR17 spectra with $T_{\rm eff} > 5000$ K and v sin $i > 8$ km s^{-1} to

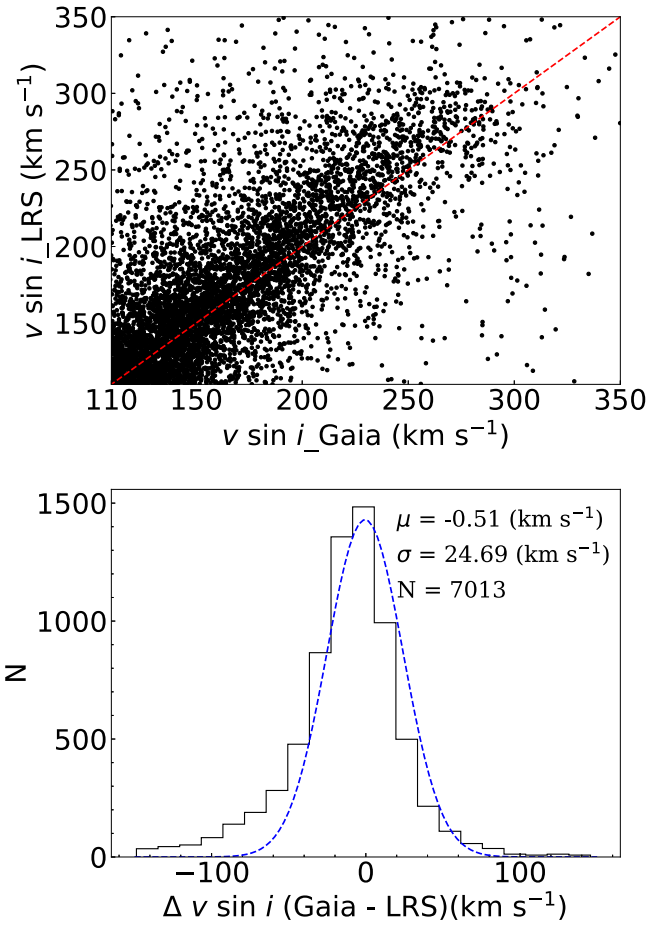

Figure 14. Comparison of the LRS v sin i to Gaia DR3 following the conventions of Figure 12.

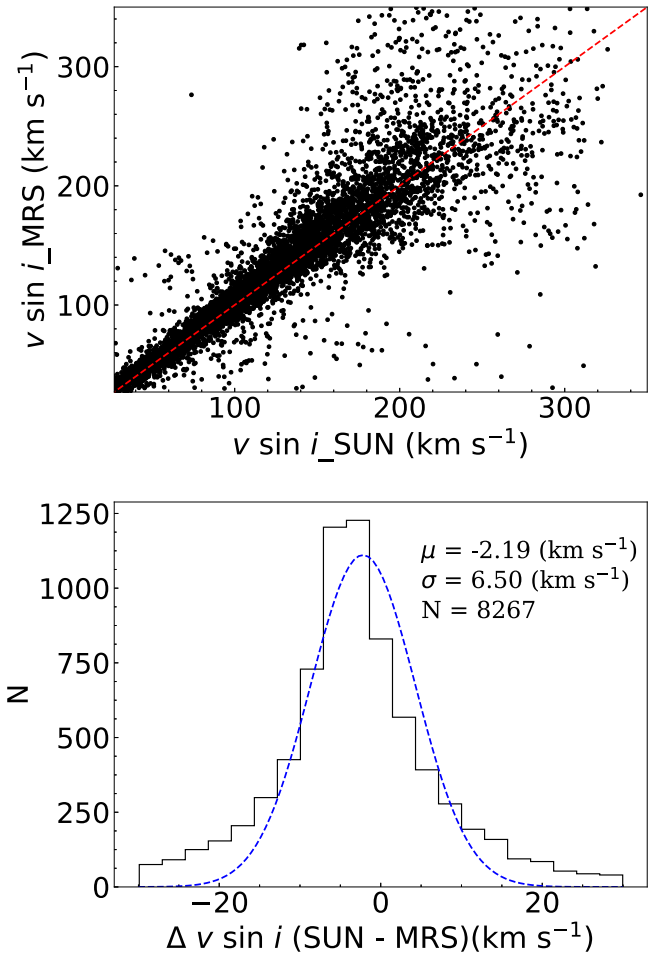

Figure 15. Comparison of the MRS v sin i to SUN following the conventions of Figure 12.

calculate their v sin i with the method proposed in this work, and the offset and scatter were 0.35 and 1.27 km s^{-1} compared to APOGEE DR17. The resolution of the APOGEE spectra were reduced to that of the LAMOST MRS spectra ($R \sim 7500$), v sin i were calculated for these spectra, and compared to the APOGEE results the offset and scatter are 3 km s^{-1} and 8.79 km s^{-1}, respectively, which indicates that the v sin i given by this work are consistent with APOGEE DR17 and that the v sin i determination method can be used for LAMOST spectra.

3. *Application to LAMOST*. We integrated the method into LASP, and applied it to both MRS and LRS spectra based on the determined atmospherical parameters of LASP. As mentioned in Frasca et al. (2016), stars with v sin $i < 27$ km s^{-1} of MRS and v sin $i < 110$ km s^{-1} of LRS were removed, and we established two v sin i catalogs, i.e., the LAMOST MRS v sin i CATALOG and the LAMOST LRS v sin i CATALOG, for 121,698 MRS stars and 80,108 LRS stars. For both MRS and LRS, the intrinsic precisions of v sin i were obtained by repeat observations, and they are $\sim$4.0 km s^{-1} for MRS and $\sim$10.0 km s^{-1} for LRS as S/N > 50. We crossmatched the two LAMOST v sin i catalogs finding that rotational velocities of 6000 common stars are consistent with an offset and scatter of 3.45 and 20.76 km s^{-1} . We found that v sin i differences of the two catalogs increase at $T_{\rm eff} > 8000$ K because the spectral lines become weaker in MRS blue-arm spectra (4950–5300 Å) when $T_{\rm eff}$ increases. The LAMOST MRS v sin i CATALOG was compared with APOGEE DR17, Gaia DR3, and SUN, respectively: v sin i in MRS are consistent with the other three catalogs and the scatters are 3.1 km s^{-1}, 12.2 km s^{-1}, and 6.5 km s^{-1}, respectively. We also compared the LAMOST LRS v sin i CATALOG with Gaia DR3 and SUN, and the v sin i scatters are 24.7 and 28.4 km s^{-1}. We noticed that the dispersion between the MRS catalog and Gaia DR3 is obviously larger than those between MRS and the other two catalogs, because Gaia only provided v sin i for hot stars and the v sin i–related information of these stars are poor in the wavelength range of 8450–8720 Å (Fouesneau et al. 2023). In addition, stars with $-0.5 \leqslant$ [Fe/H] $\leqslant 0.5$ dex in the LAMOST MRS v sin i CATALOG were selected and separated into dwarfs and giants, and we found that v sin i of both dwarfs and giants decreases as $T_{\rm eff}$ drops; the former transition occurs at $T_{\rm eff} \sim 7000$ K, and the latter occurs at 6500 K; such a result is consistent with the rotation behavior presented in Kraft (1967) and Gray (1989).

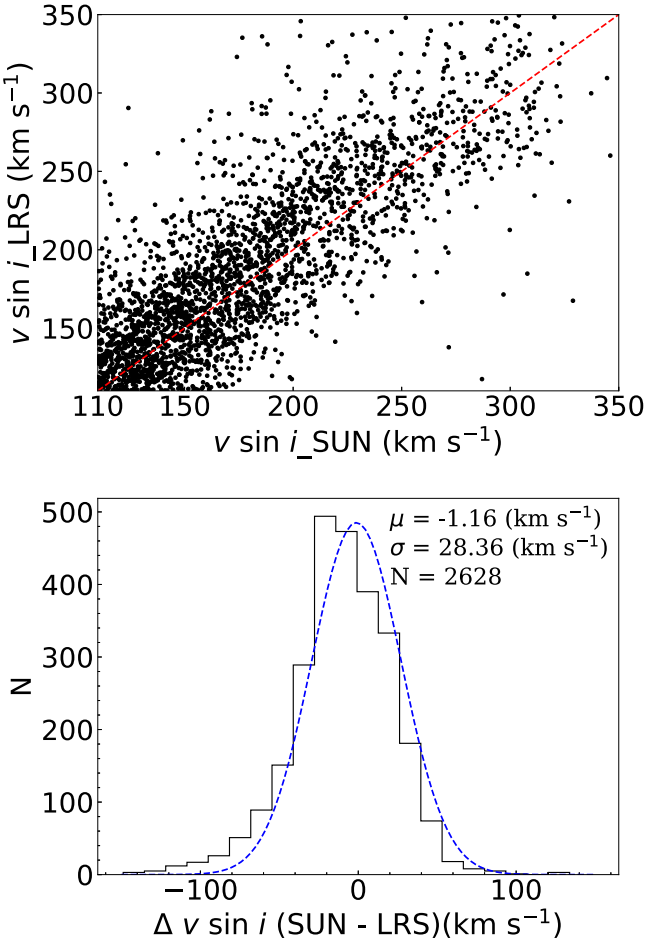

Figure 16. Comparison of the LRS v sin i to SUN following the conventions of Figure 12.

Acknowledgments

This work is supported by the National Key R&D Program of China No. 2019YFA0405502, the National Science Foundation of China (grant Nos. U1931209, 12273078 and 12073046), and the China Manned Space Project (Nos. CMS-CSST-2021-A10). We thank Hou Wen and Wang Rui for helpful discussions. Guoshoujing Telescope (the Large Sky Area Multi-Object Fiber Spectroscopic Telescope, LAMOST) is a National Major Scientific Project built by the Chinese Academy of Sciences. Funding for the project has been provided by the National Development and Reform Commission. LAMOST is operated and managed by the National Astronomical Observatories, the Chinese Academy of Sciences. This research makes use of data from the European Space Agency (ESA) mission Gaia, processed by the Gaia Data Processing and Analysis Consortium.

ORCID iDs

Fang Zuo https://orcid.org/0000-0002-9081-8951
A-Li Luo https://orcid.org/0000-0001-7865-2648
Bing Du https://orcid.org/0000-0001-6820-6441
Yinbi Li https://orcid.org/0000-0001-7607-2666
Hugh R. A. Jones https://orcid.org/0000-0003-0433-3665
Xiao Kong https://orcid.org/0000-0001-8011-8401
Yan-xin Guo https://orcid.org/0000-0002-7640-5368

References

Burkhart, C. 1979, A&A, 74, 38
Clementini, G., Ripepi, V., Leccia, S., et al. 2016, A&A, 595, A133
Creevey, O. L., Sordo, R., Pailler, F., et al. 2023, A&A, 674, A26
Cui, X.-Q., Zhao, Y.-H., Chu, Y.-Q., et al. 2012, RAA, 12, 1197
Delfosse, X., Forveille, T., Perrier, C., et al. 1998, A&A, 331, 581
Du, B., Luo, A.-L., Zhang, S., et al. 2021, RAA, 21, 202
Du, B., Luo, A.-L., Zuo, F., et al. 2019, ApJS, 240, 10
El-Badry, K., Rix, H.-W., & Heintz, T. M. 2021, MNRAS, 506, 2269
Fouesneau, M., Frémat, Y., Andrae, R., et al. 2023, A&A, 674, A28
Frasca, A., Molenda-Żakowicz, J., De Cat, P., et al. 2016, A&A, 594, A39
Fukuda, I. 1982, PASP, 94, 271
Gaia Collaboration, Brown, A. G. A., Vallenari, A., et al. 2021, A&A, 649, A1
Gaia Collaboration, Prusti, T., de Bruijne, J. H. J, et al. 2016, A&A, 595, A1
García Pérez, A. E., Allende Prieto, C., Holtzman, J. A., et al. 2016, AJ, 151, 144
Gray, D. F. 1989, ApJ, 347, 1021
Gray, D. F. 2005, The Observation and Analysis of Stellar Photospheres (3rd ed.; Cambridge: Cambridge Univ. Press)
Husser, T.-O., Wende-von Berg, S., Dreizler, S., et al. 2013, A&A, 553, A6
Jönsson, H., Holtzman, J. A., Allende Prieto, C., et al. 2020, AJ, 160, 120
Kamann, S., Bastian, N., Gossage, S., et al. 2020, MNRAS, 492, 2177
Kawaler, S. D. 1988, ApJ, 333, 236
Kounkel, M., Stassun, K. G., Hillenbrand, L. A., et al. 2023, AJ, 165, 182
Kraft, R. P. 1967, ApJ, 150, 551
Levenhagen, R. S. 2014, ApJ, 797, 29
Lu, Y., Angus, R., Foreman-Mackey, D., & Hattori, S. 2023, arXiv:2310.14990
Luo, A.-L., Zhao, Y.-H., Zhao, G., et al. 2015, RAA, 15, 1095
Melo, C. H. F., Pasquini, L., & De Medeiros, J. R. 2001, A&A, 375, 851
Nofi, L. A., Johns-Krull, C. M., López-Valdivia, R., et al. 2021, ApJ, 911, 138
Penoyre, Z., Belokurov, V., & Evans, N. W. 2022, MNRAS, 513, 5270
Recio-Blanco, A., de Laverny, P., Allende Prieto, C., et al. 2016, A&A, 585, A93
Reiners, A., & Basri, G. 2008, ApJ, 684, 1390
Royer, F., Grenier, S., Baylac, M.-O., et al. 2002, A&A, 393, 897
Schatzman, E. 1962, AnAp, 25, 18
Shang, L.-H., Luo, A.-L., Wang, L., et al. 2022, ApJS, 259, 63
Slettebak, A. 1949, ApJ, 110, 498
Slettebak, A. 1954, ApJ, 119, 146
Slettebak, A. 1955, ApJ, 121, 653
Slettebak, A., Collins, G. W., Boyce, P. B., et al. 1975, ApJS, 29, 137
Smith, M. A., & Gray, D. F. 1976, PASP, 88, 809
Su, D.-Q., & Cui, X.-Q. 2004, ChJAA, 4, 1
Sun, W., de Grijs, R., Deng, L., et al. 2019, ApJ, 876, 113
Sun, W., Duan, X.-W., Deng, L., et al. 2021, ApJS, 257, 22
Takeda, Y. 2020, PASJ, 72, 10
Wang, R., Luo, A.-L., Chen, J.-J., et al. 2019, ApJS, 244, 27
Wang, S.-G., Su, D.-Q., Chu, Y.-Q., et al. 1996, ApOpt, 35, 5155
Whiting, M. L., Hill, J. B., Bromley, B. C., et al. 2023, AJ, 165, 193
Zhang, Y.-J., Hou, W., Luo, A.-L., et al. 2022, ApJS, 259, 38
Zhao, C., & Newberg, H. J. 2006, arXiv:astro-ph/0612034
Zhao, G., Zhao, Y.-H., Chu, Y.-Q., et al. 2012, RAA, 12, 723